High photon count rate super-resolution fluorescence fluctuation spectroscopy

Falk Schneider[1*], Pablo Hernandez-Varas[2,3], B. Christoffer Lagerholm[2], Dilip Shrestha[1,] Erdinc Sezgin[1,4], M. Julia Roberti[5], Giulia Ossato[5], Frank Hecht[5], Christian Eggeling[1,2,6,7], Iztok Urbančič[1,8*]

[1]MRC Human Immunology Unit and [2]Wolfson Imaging Centre Oxford, MRC Weatherall Institute of Molecular Medicine, University of Oxford, Headley Way, Oxford, OX3 9DS, United Kingdom

[3]Core Facility for Integrated Microscopy, Panum Institute, University of Copenhagen, 2200 Copenhagen N, Denmark

[4]Science for Life Laboratory, Department of Women's and Children's Health, Karolinska Institutet, Stockholm, Sweden

[5]Leica Microsystems CMS GmbH, Am Friedensplatz 3, 68163 Mannheim, Germany

[6]Institute of Applied Optics and Biophysics, Friedrich-Schiller-University Jena, Max-Wien Platz 4, 07743 Jena, Germany

[7]Leibniz Institute of Photonic Technology e.V., Albert-Einstein-Straße 9, 07745 Jena, Germany

[8]Jožef Stefan Institute, Jamova cesta 39, SI-1000 Ljubljana, Slovenia

* corresponding authors (email: falk.schneider@rdm.ox.ac.uk, iztok.urbancic@rdm.ox.ac.uk)

Keywords: FCS, STED, high count rates, diffusion

Abstract

Probing the diffusion of molecules has become a routine measurement across the life sciences, chemistry and physics. It provides valuable insights into reaction dynamics, oligomerisation, molecular (re-)organisation or cellular heterogeneities. Fluorescence correlation spectroscopy (FCS) is one of the widely applied techniques to determine diffusion dynamics in two and three dimensions. This technique relies on the autocorrelation of intensity fluctuations but recording these fluctuations has thus far been limited by the detection electronics, which could not efficiently and accurately time-tag photons at high count rates. This has until now restricted the range of measurable dye concentrations, as well as the data quality of the FCS recordings, especially in combination with super-resolution stimulated emission depletion (STED)-FCS.

Here, we investigate the applicability and reliability of (STED-)FCS at high photon count rates (average intensities of more than 1 MHz) using novel detection equipment, namely hybrid detectors and real-time gigahertz sampling of the photon streams implemented on a commercial microscope. By measuring the diffusion of fluorophores in solution and cytoplasm of live cells, as well as in model and cellular membranes, we show that accurate diffusion and concentration measurements are possible in these previously inaccessible high photon count regimes. Other advantages include greater flexibility of experiments with biological samples with very highly variable intensity (e.g. due to a wide range of expression levels of fluorescent proteins), much shorter acquisition time, and improved data quality. This approach also pronouncedly increased the robustness of challenging live cell STED-FCS measurements of nanoscale diffusion dynamics.

Introduction

Fluorescence correlation spectroscopy (FCS) has, since its introduction almost 50 years ago, become a widely applied technique to study diffusion dynamics in synthetic and biological applications[1–3]. It has greatly contributed to the understanding of molecular diffusion in model systems and living cells, both in 2D (in vitro models or cellular membranes) and in 3D (solution or cellular cytoplasm and nucleus) environments[4–8]. Notably, it has offered fundamental insights into the dynamic organisation of living systems at the molecular level, e.g. by characterising the transient, dynamic, yet structured nature of the organisation of fluid membranes[5,9].

FCS provides a plethora of information about molecular dynamics. The diffusion rates and local concentrations of fluorescent molecules can be determined directly from the autocorrelation functions[1,10,11]. The spatial variability can be further evaluated by laser-scanning[12–14] and imaging-based variants of FCS[15–18]. Further, molecular interactions can be probed either directly, e.g. binding of molecules detected by cross-correlation (FCCS)[19], or indirectly via variations of the apparent diffusion coefficient at different length scales, measured by spot-variation FCS[20] providing information on diffusion modes as in single particle tracking[21]. Finally, the combination of FCS with super-resolution stimulated emission depletion (STED) microscopy allows direct observation of nanoscale diffusion dynamics, shedding new light on molecular organisation below the diffraction limit[22].

All these invaluable details are extracted from intensity fluctuations due to the transit of fluorescent molecules through the observation spot of the microscope. As the fluctuations (i.e. bursts in the fluorescence intensity trace) are most obvious for sparsely labelled samples, FCS is often considered a single molecule technique, and has thus been shown multiple times to perform accurately in the range of pico- and nanomolar concentrations[2]. These concentrations, though, can be far from physiological levels present in living systems, where molecular abundance can be much higher (e.g. average concentration of a protein in eukaryotic yeast cells is estimated to be around 1 μM[23]). Nevertheless, it has been theoretically predicted and experimentally verified that FCS can perform

similarly and can generate accurate results also for much larger concentrations (>100 nM)[24]. In this regime, the main factors for signal quality of FCS, often described by the signal-to-noise ratio (SNR), are the acquisition time (T), and the number of detected photons per molecule (i.e. molecular brightness, B, which depends on the absorption cross section and quantum yield of the dye, the power of the excitation laser, and the detection efficiency of the measurement setup): $\mathrm{SNR} \propto B \times T^{1/2}$ (see for example[11,25–28]).

For the most efficient and reliable detection of fluorescence fluctuations, sensitive single-photon-counting detectors are typically used, often coupled to fast electronics that enable accurate recording of photon arrival times thus also allowing additional photon filtering in post-processing[29]. One of the main drawbacks of this instrumentation, however, has been its rather long dead time after each photon detection (>100 ns)[30], limiting photon count rates to a maximum of 1 MHz. This has posed a severe limitation to the accuracy and flexibility in FCS experiments at high fluorophore concentrations, which are however unavoidable for many applications – for example when measuring binding dynamics of low affinity, or diffusion dynamics and concentrations of cellular proteins at different expression levels. Several approaches have been developed to enable FCS measurements even in such cases: labelling of only a fraction of the molecules, reduction of the simultaneously visible fluorophores via fluorescence photoswitching[31,32], splitting-up of the signal onto several detectors such as on custom-built detector banks[33], or reduction of the effective observation volume[34,35] using for example small sample containers[36], near-field structures[37,38], plasmonic near-field optics[39–41], or super-resolution STED microscopy[5,42]. Unfortunately, all of these techniques introduce more complexity and possible bias, for example due to required controls to check whether the fraction of labelled or photoswitched molecules truly reflect the entire population, influence on the sample and fluorescent molecules by surface or small volume effects, setup complexity, or perplexing photophysics of the fluorescent label.

Here, we demonstrate the straightforward realisation of FCS measurements at high photon count rates on a commercially available microscope, using novel photon counting instrumentation. By measuring the diffusion of fluorescent dyes in solutions, artificial and cell membranes, we explore performance, capabilities, accuracy, applicability and limitations of confocal FCS and STED-FCS experiments at photon count rates of up to 20–30 MHz per detection channel, revealing great potential for FCS experiments at high count rates. As examples, we show the independence of cytosolic protein diffusion on cellular expression levels and the application of high count rates to STED-FCS measuring the diffusion behaviour of lipids in cellular plasma membranes.

Results and Discussion

Non-saturated photon detection at high dye concentrations and laser excitation powers

We first tested the advanced photon counting instrumentation, implemented on a confocal and STED-capable microscope, by recording fluorescence fluctuation data from a single dye (Atto655) diffusing in aqueous solution at different concentrations or excitation laser powers, resulting in different photon count rates. The photon counting instrumentation included hybrid detectors with very short dead times and fast FPGA electronics with real-time GHz sampling and pattern matching, which together with the 80 MHz pulsed fluorescence excitation allows for detection of photon count rates of tens of MHz without corrections (as described in detail in the Materials and Methods section). Figure 1A and B show fluctuations in the normalized photon count rates over time as recorded for three different dye concentrations and laser excitation powers, respectively. As expected from theory[10,25–28], the relative fluctuations around the average count rate decrease with increasing dye concentration, but much less so with excitation laser power. Most importantly, we could follow a linear increase of photon count rate with dye concentration and laser excitation power (Figure 1C and D), as expected in the absence of limitations in detection electronics. Note that approximate linearity was maintained despite employing dye concentrations of up to 1 µM and registering photon count

rates of up to 20-30 MHz. The non-linearity introduced at excitation laser powers larger than 40 µW (≈ 30 kW/cm², Figure 1D) were to be expected due to dye photobleaching and saturation of excited state population and consequently fluorescence emission (i.e. not due to detector saturation, compare Figure 1C at same count rate levels), while slight saturation effects at very high dye concentrations may result from photon re-absorption and dye self-quenching, as indicated previously[33,43]. In due consideration of acquisition count rate being the limiting factor in conventional equipment, we present the rest of the data as a function of this parameter.

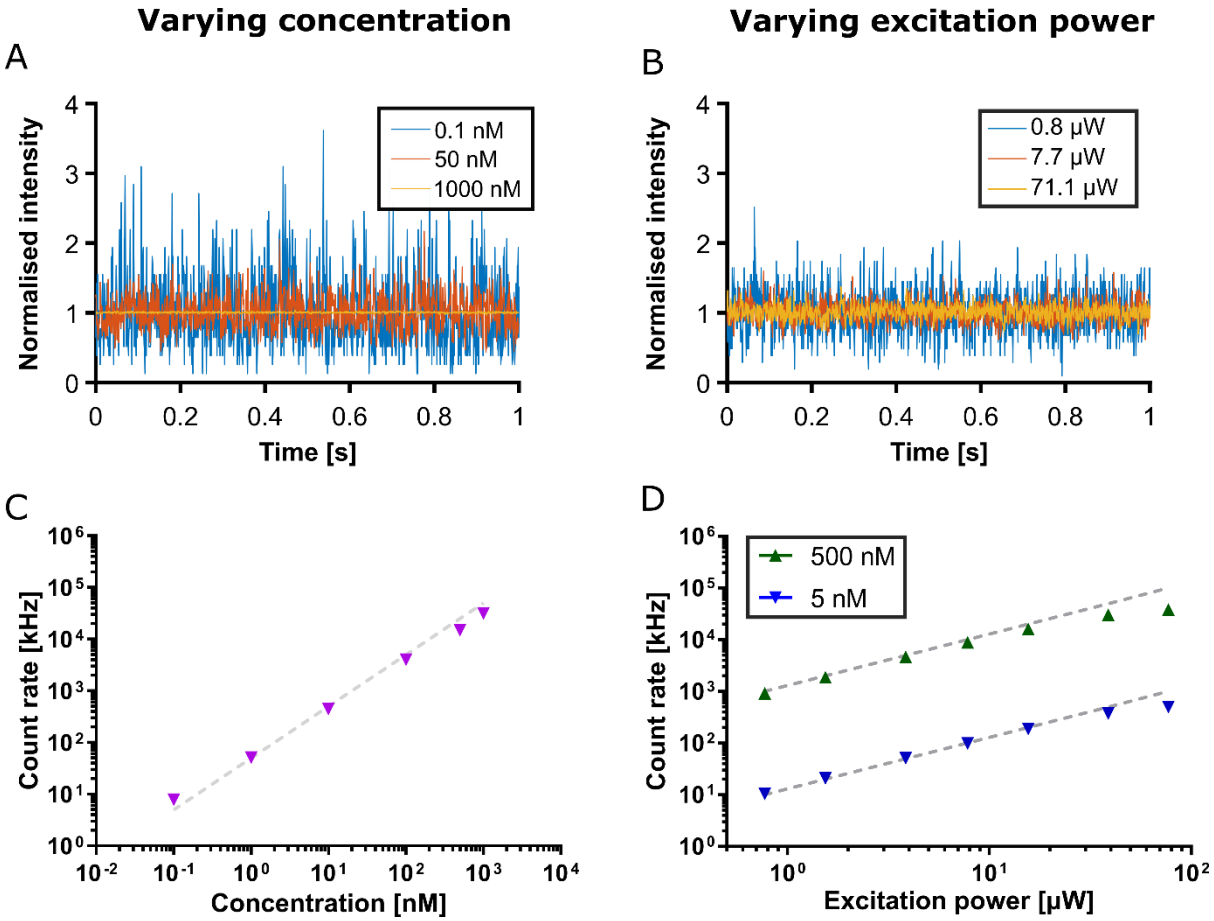

Figure 1: Influence of varying concentration and photon count rates on FCS measurements of the dye Atto655 in aqueous solution. **A,B** Normalized detected photon count rate data (intensity) over time at different dye concentrations (A, 0.1 nM, 50 nM, and 1 µM as labelled; excitation laser power 15.4 µW) and excitation laser powers (B, as labelled; concentration 5 nM), highlighting the reduction in relative intensity fluctuations for higher concentrations and excitation laser powers. **C,D** Detected photon count rates versus instituted dye concentration (C, dashed lines indicate the expected linear increase; excitation laser power 15.4 µW) and

instituted excitation laser power for 5 nM (blue) and 500 nM (green) (D, dashed lines indicate the expected linear increase). Values are averages of three repetitions (acquisition time 15 s each), and standard deviations are smaller than the size of the symbols.

FCS noise levels at different count rates

The ability to record photon time traces at high count rates consequently allowed us to acquire FCS data for Atto655 up to 1 µM high dye concentrations and excitation laser powers up to 40 µW (≈ 30 kW/cm²). The autocorrelation curves for these unconventional conditions show similar decays as for low dye concentrations and laser powers (Figure 2A and B). From the common FCS theory excluding concentration or saturation effects, average transit times should be independent of dye concentration and laser power, while the amplitude of the autocorrelation curve should linearly decrease with dye concentration and stay constant with laser power, which we could well recover from fitting our FCS data, even when recorded at count rates of up to 20-30 MHz (Figure 2C and D). As before, deviations at the highest tested laser powers > 40 µW can be attributed to dye photobleaching and fluorescence emission saturation.

An interesting feature of the FCS data recorded at different dye concentrations or excitation laser powers, i.e. photon count rates, are the different noise levels and resulting data quality. From theory[11, 24,26], the noise in FCS data should linearly decrease with excitation laser power and be independent of dye concentration. The latter has for example been experimentally verified for dye concentrations of up to around 100 nM[24]. Consequently, we set out to investigate noise levels for FCS data recorded at the large dynamic range of dye concentrations and laser powers, which became accessible using the new equipment.

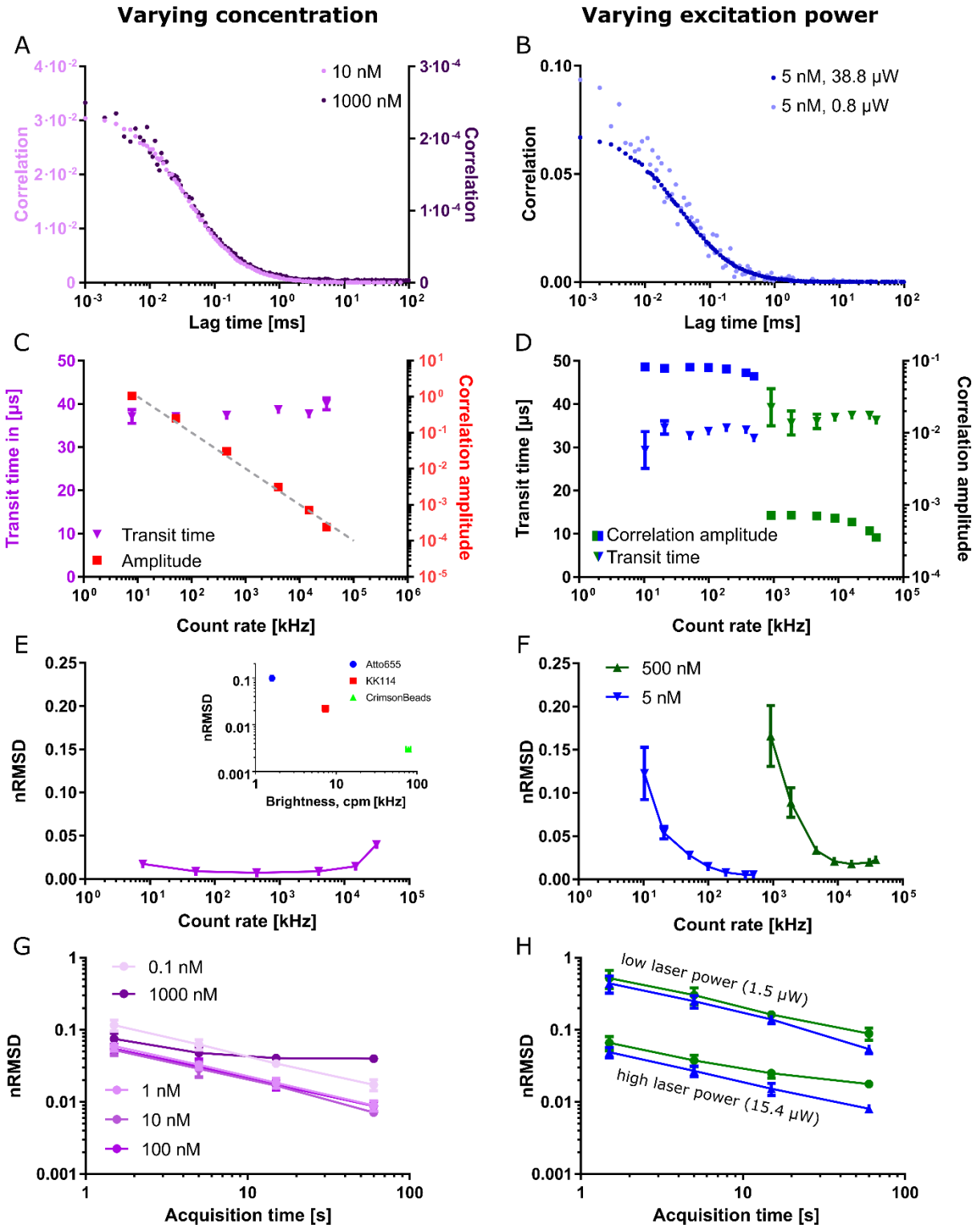

Figure 2: Detailed analysis of the FCS data of Atto655 in aqueous solution at varying instituted dye concentration c_{dye} (left panels) and excitation laser power P_{laser} (right panels). **A,B** Representative FCS curves at different concentrations (A, as labelled, P_{laser} = 15.4 µW) excitation laser powers (B, as labelled, c_{dye} = 5 nM). **C-F** Transit time, correlation amplitude (C and D, axes and colours as labelled), and nRMSD (i.e. noise in correlation data, E and F; F: for two c_{dye} as labelled) as determined from FCS for different photon count rates, i.e. different c_{dye} (C, E) and P_{laser} (F, G). (**Inset E**) Values of nRMSD as determined from FCS for different dyes in aqueous solution with

different brightness, i.e. counts-per-molecule (cpm) (average over c_{dye} ≈ 0.01–1 µM or 1:100–1:2000 dilutions of the stock bead suspension (see Figure SI 3), P_{laser} = 1.5 µW). **G,H** Values of nRMSD as determined from FCS data of Atto655 at different acquisition times and at varying c_{dye} (G, P_{laser} = 15.4 µW) and P_{laser} (H, c_{dye} = 5 or 500 nM) as labelled. Data points represent averages and standard deviations (unless smaller than the symbols) of three repetitions (60 s acquisition time if not indicated otherwise).

Already visual inspection of our FCS data recorded at the different conditions (Figure 2A and B) indicated notable differences in noise levels, especially for the different excitation laser powers (shown as the spread of the correlation curve, most pronounced at short lag times). We evaluated the noise by calculating the root-mean-square of the fitting residuals normalized to the amplitude (nRMSD), with lower values indicating better data quality (see Methods and Figure SI 1 for details). This provides us with a single value for the data quality of each measurement. Conveniently, this measure roughly corresponded to the relative standard deviation of the values of average transit times determined from fitting of the data (Figure SI 2, the nRMSD relates closely to the measurement error). In accordance with the theoretical predictions[11, 24,26], the nRMSD was only weakly affected by varying concentration (Figure 2E), but could be greatly improved by increased excitation laser power (Figure 2F). The excitation laser power directly increases the dyes' excited state population and thus fluorescence emission rate and the average detected count rate per single dye (molecular brightness), which is the reason for the improvements in noise levels. Under comparable measurement conditions, the nRMSD is therefore also a direct indicator of the molecular brightness of the investigated dye (inset in Figure 2E and Figure SI 3). Deteriorated noise levels, i.e. higher nRMSD values, were again observed at dye concentrations around 1 µM, but were much less pronounced at the highest excitation laser powers above 20–40 µW, despite detected saturation of photon count rates (Figure 1D) and deviations of values of the transit times and correlation amplitudes (Figure 2D) as highlighted above.

FCS noise levels at different acquisition times

Predicted from theory and to a certain extent verified experimentally[11, 24,26], the noise in FCS data should decrease with the square root of the acquisition time. We could well reproduce this dependence for different dye concentrations and excitation laser powers (Figure 2G and H; again, the same issues as outlined above caused deviations at high dye concentrations and excitation laser powers). This data establishes unique possibilities of adapting to experimental conditions. Due to the absence of saturation effects in photon count rates in the 5–500 nM concentration range, the possibility of increasing the laser power and detecting correspondingly higher photon count rates does not only increase the data quality (i.e. lower nRMSD values), but alternatively allows for a significant reduction (up to two orders of magnitude) in the acquisition time required for generating similar data quality (Figure 2G and H, Figure SI 2).

FCS of cytosolic GFP in live cells at various expression levels

The possibility of acquiring accurate FCS data in a wide range of dye concentrations allows simplification or realization of experiments under challenging conditions. For example, FCS-based measurements of diffusion or concentration of fluorescent proteins in cells are usually challenged by the naturally varying expression levels of the fluorescent proteins, as shown in the confocal image in Figure 3A for HeLa cells expressing cytoplasmic GFP (green fluorescent protein). Using standard FCS instrumentation, only carefully chosen dim cells would be measurable, which may represent only a small, and not necessarily representative fraction of all cells, introducing a potential source of bias.

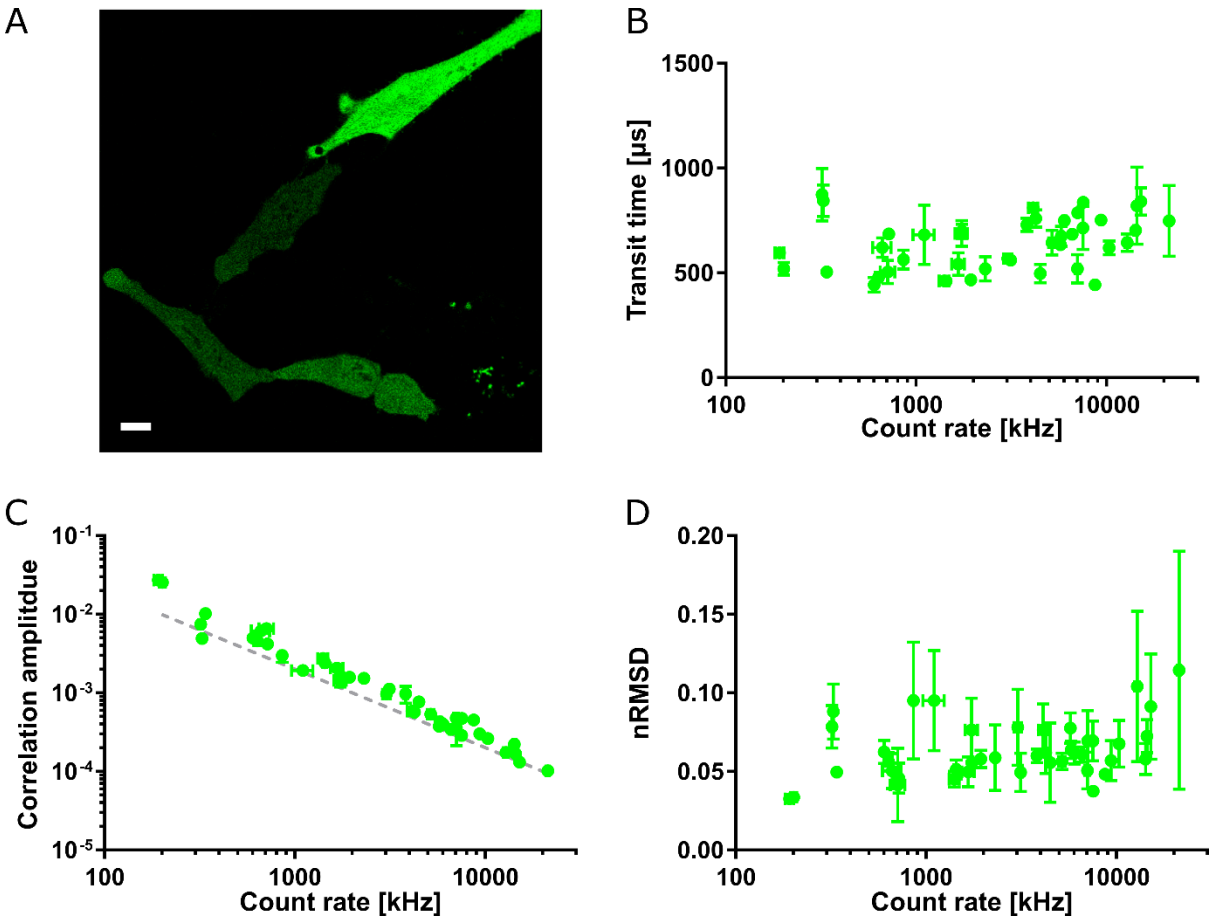

Figure 3: Acquiring FCS data in live cells at different expression levels of the fluorescent protein GFP-SNAP. **A** Representative confocal image of HeLa cells transiently transfected with cytoplasmic GFP-SNAP, highlighting different brightness and thus expression levels. **B-D** Values of transit time (B), correlation amplitude (C), and nRMSD (i.e. noise in correlation data, D) as determined from FCS for different photon count rates, i.e. different expression levels. Averages and standard deviations of at least three measurements per cell (15 s, 0.6 µW excitation laser power).

Using our current setup, we could now record FCS data for all HeLa cells irrespective of their fluorescence intensity, revealing average transit times of GFP over a wide range of photon count rates and thus concentrations resulting from different expression levels (Figure 3B). The photon count rates are correlated with the correlation amplitude (Figure 3C), which is inversely proportional to the average number of fluorescent molecules in the observation volume (see Materials and Methods) and thus concentration and expression level of GFP can be inferred. Taking our observation volume of about 1 fL, we can estimate concentrations of GFP of approx. 0.01–5 µM between the differently

expressing cells (see Materials and Methods). These data indicate that within the tested range the mobility of GFP is independent of expression level. In addition, the quality of the FCS data as quantified by the nRMSD values was maintained over the range of tested expression levels (Figure 3D), as predicted from the behaviour of the organic dye in solution (compare Figure 1). Only in the regime beyond 10 MHz (in our case corresponding to concentrations around 1 µM), we observed notable signal deterioration.

STED-FCS of lipid dyes in model membranes

The main strength of FCS on a super-resolution STED microscope, STED-FCS, is the ability to directly report on nanoscale molecular mobility and thus determine apparent values of diffusion coefficients from the average transit times (see Materials and Methods) for different observation spot sizes – from conventional confocal spot sizes with lateral diameters of around 200 nm, down to STED microscopy recordings with observation spot diameters of 30 – 40 nm. From the dependency of the apparent values of the diffusion coefficient on the observation spot diameter, STED-FCS has provided insights into the molecular diffusion modes, similar to spot-variation FCS[20], but now at the relevant molecular scale, which is particularly valuable for the elucidation of the nanoscale architecture of biological membranes[22]. However, measurements at various sizes of the effective observation spot inherently impose a large variation in the average number of fluorescent molecules in the observation spot (N) and thus detected photon count levels (Figure 4A, schematics). Large observation spots at the confocal recordings entail already high count rates and high values of N at rather low dye concentrations, while the smaller observation spots at the STED microscopy recordings require relatively large dye concentrations to reach photon count rates and values of N that are high enough for allowing reasonably low acquisition times (it has also been shown theoretically that too low count rates or concentrations lead to noisy and inaccurate FCS data[11, 24,26]). This has limited the range of useful dye concentrations in STED-FCS measurements using conventional detection electronics.

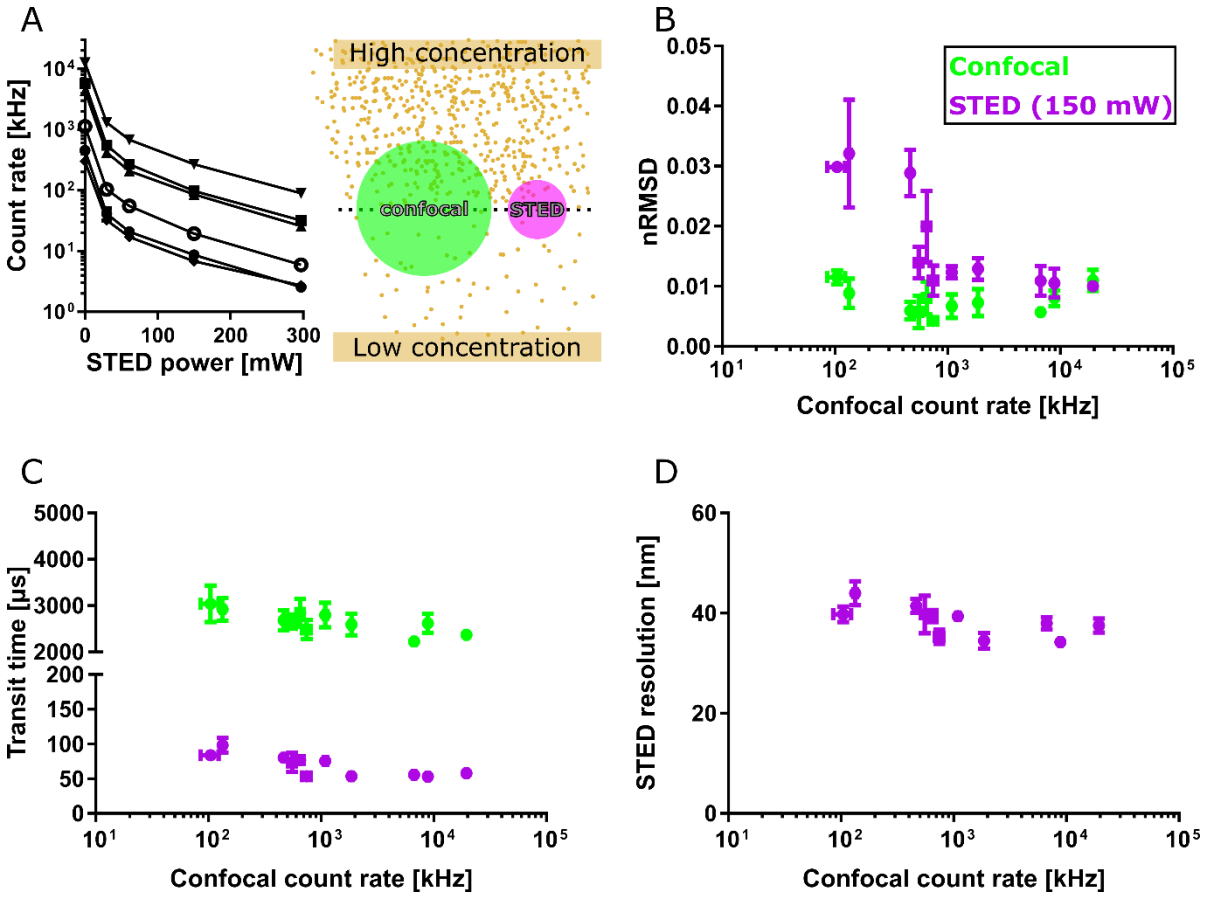

Figure 4: STED FCS in supported lipid bilayers (SLBs) at various dye concentrations. **A right** Sketch illustrating the shrinking of the confocal observation spot (green) to the STED focus (purple) for a high or low concentration of dye molecules (yellow dots) **Left** Fluorescence intensity for multiple DOPC SLBs with various concentrations of fluorescent lipid dye Abberior STAR Red-DPPE after depletion with different STED laser powers. From these data, the noise level of FCS data (nRMSD, **B**), the average fitted transit time (**C**), and calculated apparent STED resolution (**D**), were plotted against confocal acquisition count rates, for confocal (green) and STED FCS recordings (purple, 150 mW depletion power). Excitation power 2.3 µW, acquisition time 15 s. Each data-point represents the average and standard deviation of at least three measurements per SLB preparation.

To evaluate the performance of the new detection electronics in STED-FCS, we recorded data at varying concentrations of the fluorescent lipid analogue Abberior STAR Red-DPPE diffusing in a fluid supported lipid membrane bilayer (SLBs), which is a convenient and well characterised model membrane system, often used as a control sample in STED-FCS experiments[22]. While increasing the

lipid analogue concentration and pushing the confocal count rates beyond the conventional FCS range (Figure 4A) did not influence the noise in confocal measurements (Figure 4B, green data points), it - as expected - significantly improved the data quality of the STED-FCS recordings (low nRMSD values, Figure 4B, purple data points). Also as expected from theory, the values of transit times were smaller in the STED compared to the confocal recordings (due to the reduced observation spot size in the STED mode, here roughly 40 nm in diameter) and hardly changed with concentrations of the fluorescent probe (i.e., at increased count rate, Figure 4C). Similarly, the observation spot diameters as determined from the recorded FCS data remained constant (Figure 4D, see Methods for details about its calculation), all in all highlighting the great flexibility and improvement in STED-FCS experiments when employing non-saturating detection electronics.

For simplicity, we demonstrated the above effects at a single STED laser power (150 mW, observation spot diameter of 40 nm), but the conclusions held also true for other STED laser powers (and thus observation spot sizes). Similar or even larger improvements of STED-FCS data quality as by increasing the dye concentration were achieved by increasing the excitation laser power (Figure SI 4), supporting the benefits of high count rates for STED-FCS experiments.

STED-FCS in live cell membranes

Finally, we verified the reliability of STED-FCS measurements at high photon count rates for measurements in living cells. We labelled the plasma membrane of live HeLa cells using the fluorescent lipid analogue Cholesterol-PEG-Abberior STAR Red (Chol-PEG-KK114) (Figure 5A), for which previous studies have consistently indicated free diffusion in cellular plasma membranes[44]. The resulting STED-FCS data show low nRMSD values, i.e. low noise levels in the correlation data, which can in the STED microscopy mode be significantly improved to almost confocal quality by increasing either the excitation laser power or concentration of Chol-PEG-KK114 (i.e. total count rate, Figure 5B) without biasing the resulting values of transit times (Figure 5C).

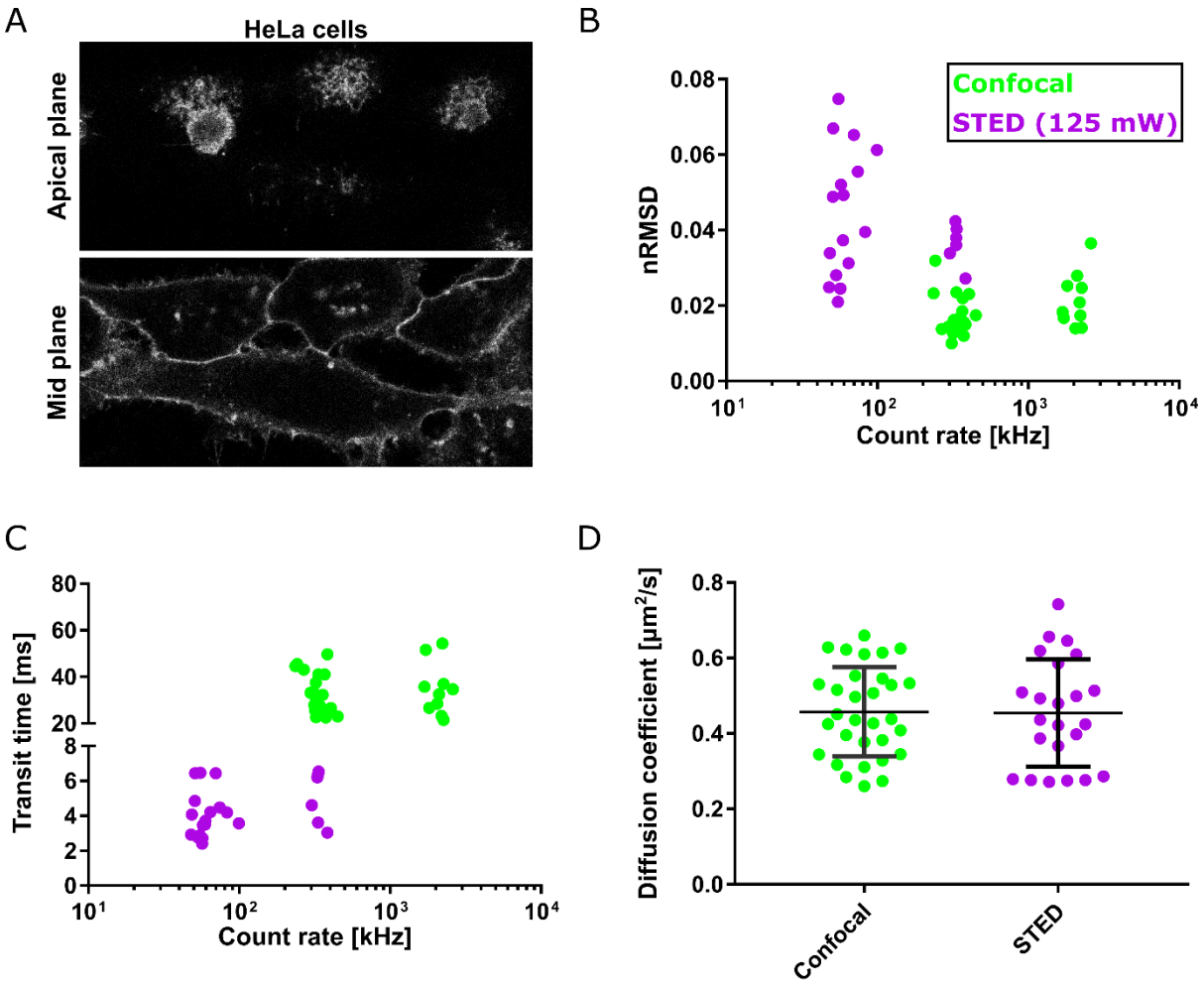

Figure 5: STED-FCS of Abberior STAR-Red-PEG-Cholesterol in membranes of live HeLa cells. **A** Confocal image of the top plane (roughly 10 µm above the cover slip) and mid plane of HeLa cells, membrane labelled with the fluorescent cholesterol analogue (image sizes 60 × 27 µm^2) **B** The noise level of FCS data (nRMSD values) and **C** average fitted transit time for confocal (green) and STED-FCS recordings (125 mW depletion laser power, purple), in the top membrane of HeLa cells, plotted against their respective count rates. **D** Diffusion coefficient determined from FCS data in confocal and STED mode in the top membrane of the HeLa cells. Every dot represents a single FCS measurement. Excitation laser 2.3 µW, acquisition time 15 s.

Note that we here measured the diffusion in the apical membrane of HeLa cells, i.e. 5-10 µm above the microscope coverslip (Figure 5A), rather than in the basal membrane as before[44]. This avoids potential biasing effects by the coverslip surface. Yet, penetration through the aqueous cellular environment over such a distance causes spherical aberrations when employing a traditional oil-immersion STED microscope objective (due to the refractive index mismatch between water and oil)[45],

having detrimental effects on STED-FCS experiments (Figure SI 5). Such aberrations can either be corrected for using adaptive optics[46,47] or employing a water immersion objective[48], which shows constant signal levels and performance of for example STED and STED-FCS experiments in a wide range of focal depths (5-100 µm above the coverslip) without the need for depth-dependent readjustments of the correction collar (Figure SI 5). Taking the observation spot size as determined from calibration data (Figure SI 6, diameter of 100 nm), we could calculate apparent values of the diffusion coefficient D for both the confocal and STED mode (spot diameters of 280 and 100 nm, respectively; see Materials and Methods), which were both in the same range (D ≈ 0.45 µm²/s, Figure 5D) as observed before for the basal membrane[44], highlighting free diffusion and indicating similar diffusion characteristics of the probe in the apical and basal plasma membrane[44], i.e. negligible bias by the coverslip surface.

Conclusions

We systematically evaluated the reduction in error and bias of FCS measurements recorded at high photon count rates, as enabled by novel detection electronics integrated into a turn-key microscope. We were able to record highly accurate FCS data with detected photon count rates of up to about 10 MHz, i.e. dye concentrations up to 1 µM. This improved performance introduces huge flexibility for performing FCS experiments to measure diffusion or concentration, previously impossible due to limitations in the detection electronics (allowing e.g. only recordings of photon count rates of up to 0.8–1 MHz). This now enables: 1) FCS measurements at high dye concentrations for e.g. low-affinity binding assays, 2) the recording of fluctuation data with reduced acquisition times by increasing the excitation power to higher count rates, 3) performing live-cell experiments in a wide range of expression levels of fluorescently tagged proteins, and 4) optimization of the data quality of STED-FCS recordings over a wide range of observation spot sizes by increasing dye concentration and/or excitation laser power. Using these features we could for example show that cytosolic diffusion of GFP

was independent of expression level in live HeLa cells, and that the fluorescent lipid analogue was diffusing freely in the apical membrane similarly as reported before for the basal membrane[44]

Improved detection instrumentation as the one presented here are becoming increasingly available and will be further optimized, pushing the ease of use of FCS or related measurements, such as fluorescence cross correlation spectroscopy (FCCS)[49], fluorescence lifetime correlation spectroscopy (FLCS)[50], number and brightness (N&B) analysis[51], or line- and raster-scanning correlation spectroscopy (RICS)[12,52]. In combination with high-throughput methods this could enable the systematic evaluation of overexpression of fluorescent proteins[53], tracking of dynamically changing diffusion properties, or other previously unattainable applications.

Acknowledgements

The authors thank for the funding from MRC Proximity to Discovery funds (MC_PC_16082 (P2D Technologies 2 Therapies)), Marie Skłodowska-Curie Actions (707348; I.U.), Newton-Katip Celebi Institutional Links grant (352333122, E.S.), Medical Research Council (MC_UU_12010/unit programs G0902418 and MC_UU_12025), MRC/BBSRC/EPSRC (MR/K01577X/1), Wolfson Foundation, Wellcome Trust (104924/14/Z/14), Deutsche Forschungsgemeinschaft (Research unit 1905, Excellence Cluster Balance of the Microverse, Collaborative Research Centre 1278 Polytarget), Wellcome Institutional Strategic Support Fund, and Oxford internal funds (EPA Cephalosporin Fund and John Fell Fund), support from the Micron Oxford Advanced Bioimaging Unit (Wellcome Trust funding 107457/Z/15/Z), and Dr. Katharina Reglinski for kindly providing the GFP-SNAP plasmids.

Conflict of interest

The authors declare no conflict of interest but need to note that MJR, GO and FH are employed at Leica Microsystems which manufactures and sells the SP8 STED FALCON used throughout the study.

Materials and Methods

Preparation of dyes in solution

Atto655 NHS-ester (AttoTec), Abberior STAR Red NHS-ester also termed KK114 (Abberior), and 20-nm crimson beads (Thermofisher) were stored at concentration >10 µM and diluted in PBS for measurements.

Preparation of Supported Lipid Bilayers (SLBs)

SLBs were prepared by spin coating as described previously[54]. Briefly, a solution of 1 mg/mL DOPC (1,2-dioleoyl-sn-glycero-3-phosphocholine, Avanti Polar Lipids) dissolved in 1:2 Methanol:Chloroform was coated at 3200 rpm for 45 seconds on a 25 mm diameter cover slip. The formed lipid film was rehydrated with SLB buffer (150 mM NaCl, 10 mM HEPES, pH 7.4) and washed several times. All cover slips for SLB preparation were piranha cleaned (3:1, H_2S0_4:H_2O_2) and stored in water. SLBs were labelled with varying amounts of Abberior STAR Red-DPPE (1,2-dipalmitoyl-sn-glycero-3-phosphoethanolamine, Abberior).

Tissue Culture

HeLa cells were cultured at 37 °C at 5% CO_2 in high-glucose DMEM (Thermofisher) supplemented with 10 % FBS (Thermofisher), L-Glutamine (Thermofisher) and penicillin/streptomycin (Thermofisher). Cells were seeded onto 35 mm IBIDI glass bottom dishes coated with fibronectin (10 µg/mL for 5 min and washed with PBS) 24 h prior to performing the measurements.

CHO K1 cells were grown at 37 °C at 5% CO_2 in DMEM/F12 (Lonza) supplemented with 10 % FBS (Sigma) and L-Glutamine (Sigma).

The transfections of GFP-SNAP, cytoplasmic GFP, obtained from Dr. Katharina Reglinski, were performed with Turbofect (ThermoFisher) according to the manufacturer's protocol.

Preparation of Giant Plasma Membrane Vesicles (GPMVs)

GPMVs were prepared as described previously[54,55]. In brief, HeLa cells were cultured as described above but seeded on 35 mm plastic bottom petri dishes. At a confluency of about 75 % , the cells were washed with GPMV buffer (150 mM NaCl, 2 mM $CaCl_2$, 10 mM HEPES, pH 7.4) and then incubated with 25 mM PFA and 10 mM DTT in GPMV buffer for 2 h at 37 °C. The GPMV containing supernatant was collected and labelled with Abberior STAR Red-PEG(2kDA)-Cholesterol (Abberior) at a final concentration of 0.5 μg/mL for 10 minutes. GPMVs were non -specifically immobilised on poly-*L*-lysine (PLL) coated surfaces as described before[14]. All diffusion measurements in GPMVs were performed on the top membrane.

Instrumentation & microscopy

All experiments were performed on a Leica SP8 STED FALCON (Leica Microsystems) equipped with the HC PL APO 100x/1.40 Oil STED WHITE oil immersion objective lens (SLB measurements) and the HC PL APO 86x/1.20 W motCORR STED WHITE water immersion objective lens with a motorised correction collar (for solution, cytosolic, and apical cell membrane measurements). The STED WHITE 86x water lens has a working distance of 300 μm, and the motorised correction collar adjusts for refraction index mismatch by optimizing the signal for every sample (coverslip). It is worth noting that a single initial setting of the correction collar was sufficient to correct for varying depth over the investigated range of 100 μm (compare Figure SI 5). We used the 488-nm and 633-nm lines of a white light laser as the excitation source. STED-FCS experiments were performed using a 775 nm pulsed laser (80 MHz) for depletion with laser powers between 0 and 300 mW measured at the objective. The respective notch

filters (775 nm, 633 nm or 488 nm) were used for emission clean up. For all measurements with constant excitation power we stayed below saturation intensity (by checking proportionality of excitation laser power and fluorescence intensity) as triplet pumping may result in an additional source of deviations[56].

All FCS experiments were performed using the hybrid detectors (HyD-SMDs), featuring very short dead times, and FALCON electronics allowing acquisition of TCSPC data at photon count rates of up to 80 Mcps per detection channel without the necessity for corrections. This implementation is based on sampling the signal from the pulsed laser and detectors using fast FPGA electronics and applying pattern matching to the resulting bitstreams, producing as output the photon arrival times with a resolution of 97 ps and deadtime <1.5 ns, at GHz sampling rates.

Measurement times ranged as indicated from 10 to 60 seconds. Only for the lifetime measurements we used 40 MHz pulsing of the white light laser for excitation.

Data analysis

Correlation, time trace cropping, gating and fitting was performed using the built-in routines in LAS-X (Leica Microsystems). Time gates were applied as appropriate; most importantly in STED-FCS to remove confocal contributions (see Figure SI 7). Fitted curves, intensity traces and fitting parameters were exported to Excel (Microsoft) for further analysis. Solution and cytoplasmic GFP data were fitted with a free 3D diffusion model (including offset and triplet as appropriate: triplet time GFP 40 µs, Atto655 none[57], Abberior STAR Red 5 µs). SLB, GPMV and cell membrane data were fitted with a 2D diffusion model (including offset and triplet time for Abberior STAR Red-PEG-Chol: 5 µs).

For concentration estimation we assume a confocal volume of 1 fL. Given that the amplitude relates to the inverse number of particles, concentrations can be estimated[10].

As a measure of data quality and curve smoothness, nRMSD values were calculated by taking the root-mean-square difference between the measured FCS curve and its fit up to the transit time, and normalised to the fitted amplitude. For STED-FCS experiments the diffusion coefficient was calculated as described before[22] using the following formula:

$$D = \frac{\omega^2}{8 \cdot \ln(2) \cdot \tau_D}$$

Where D is the apparent diffusion coefficient (in confocal or STED), ω^2 refers to the full width half max (FWHM) of the observation spot (in confocal or STED) and τ_D to the transit time extracted from the FCS fit. The FWHM was determined by confocal and STED imaging of fluorescent beads (20 nm crimson beads). Using the assumption that the fluorescently labelled lipids diffuse freely in a SLB, the FWHM can be calculated as a function of STED power using the following equation[22]:

$$\omega(STED) = \omega(confocal) \cdot \sqrt{\left(\frac{\tau_{D,STED}}{\tau_{D,confocal}}\right)}$$

Note that we used the top membrane of immobilised GPMVs labelled with Abberior STAR Red-PEG-Cholesterol to determine the FWHM far away from the surface using a water immersion objective.

References

(1) Magde, D.; Elson, E.; Webb, W. W. Thermodynamic Fluctuations in a Reacting System—Measurement by Fluorescence Correlation Spectroscopy. *Phys. Rev. Lett.* **1972**, *29*, 705–708.

(2) Elson, E. L. Fluorescence Correlation Spectroscopy: Past, Present, Future. *Biophys. J.* **2011**, *101*, 2855–2870.

(3) Ehrenberg, M.; Rigler, R. Rotational Brownian Motion and Fluorescence Intensify Fluctuations. *Chem. Phys.* **1974**, *4*, 390–401.

(4) Cebecauer, M.; Amaro, M.; Jurkiewicz, P.; Sarmento, M. J.; Šachl, R.; Cwiklik, L.; Hof, M. Membrane Lipid Nanodomains. *Chem. Rev.* **2018**, *118*, 11259–11297.

(5) Sezgin, E.; Levental, I.; Mayor, S.; Eggeling, C. The Mystery of Membrane Organization: Composition, Regulation and Roles of Lipid Rafts. *Nat. Rev. Mol. Cell Biol.* **2017**, *18*, 361–374.

(6) Di Bona, M.; Mancini, M. A.; Mazza, D.; Vicidomini, G.; Diaspro, A.; Lanzanò, L. Measuring Mobility in Chromatin by Intensity-Sorted FCS. *Biophys. J.* **2019**, *116*, 987–999.

(7) Lanzanò, L.; Scipioni, L.; Di Bona, M.; Bianchini, P.; Bizzarri, R.; Cardarelli, F.; Diaspro, A.; Vicidomini, G.; Bona, M. Di; Bianchini, P.; Bizzarri, R.; Di Bona, M.; Bianchini, P.; Bizzarri, R.; Cardarelli, F.; Diaspro, A.; Vicidomini, G.; Bona, M. Di; Bianchini, P. et al. Measurement of Nanoscale Three-Dimensional Diffusion in the Interior of Living Cells by STED-FCS. *Nat. Commun.* **2017**, *8*, 65.

(8) Eggeling, C.; Hellriegel, C. Editorial. *Methods* **2018**, *140–141*, 1–2.

(9) Jacobson, K.; Liu, P.; Lagerholm, B. C. The Lateral Organization and Mobility of Plasma Membrane Components. *Cell* **2019**, *177*, 806–819.

(10) Lackowicz, J. *Principles of Fluorescence Spectroscopy*, Third.; Lakowicz, J. R., Ed.; Springer US: Boston, MA, 2006.

(11) Koppel, D. E. Statistical Accuracy in Fluorescence Correlation Spectroscopy. *Phys. Rev. A* **1974**, *10*, 1938–1945.

(12) Ruan, Q.; Cheng, M. A.; Levi, M.; Gratton, E.; Mantulin, W. W. Spatial-Temporal Studies of Membrane Dynamics: Scanning Fluorescence Correlation Spectroscopy (SFCS). *Biophys. J.* **2004**, *87*, 1260–1267.

(13) Ries, J.; Chiantia, S.; Schwille, P. Accurate Determination of Membrane Dynamics with Line-Scan FCS. *Biophys. J.* **2009**, *96*, 1999–2008.

(14) Schneider, F.; Waithe, D.; Lagerholm, B. C.; Shrestha, D.; Sezgin, E.; Eggeling, C.; Fritzsche, M. Statistical Analysis of Scanning Fluorescence Correlation Spectroscopy Data Differentiates Free from Hindered Diffusion. *ACS Nano* **2018**, *12*, 8540–8546.

(15) Rossow, M. J.; Sasaki, J. M.; Digman, M. a; Gratton, E. Raster Image Correlation Spectroscopy in Live Cells. *Nat. Protoc.* **2010**, *5*, 1761–1774.

(16) Sankaran, J.; Manna, M.; Guo, L.; Kraut, R.; Wohland, T. Diffusion, Transport, and Cell Membrane Organization Investigated by Imaging Fluorescence Cross-Correlation Spectroscopy. *Biophys. J.* **2009**, *97*, 2630–2639.

(17) Jin, W.; Simsek, M. F.; Pralle, A. Quantifying Spatial and Temporal Variations of the Cell Membrane Ultra-Structure by BimFCS. *Methods* **2018**, *140–141*, 151–160.

(18) Hebert, B.; Costantino, S.; Wiseman, P. W. Spatiotemporal Image Correlation Spectroscopy (STICS) Theory, Verification, and Application to Protein Velocity Mapping in Living CHO Cells. *Biophys. J.* **2005**, *88*, 3601–3614.

(19) Schwille, P.; Meyer-Almes, F. J.; Rigler, R. Dual-Color Fluorescence Cross-Correlation Spectroscopy for Multicomponent Diffusional Analysis in Solution. *Biophys. J.* **1997**, *72*, 1878–1886.

(20) Wawrezinieck, L.; Rigneault, H.; Marguet, D.; Lenne, P.-F. Fluorescence Correlation Spectroscopy Diffusion Laws to Probe the Submicron Cell Membrane Organization. *Biophys. J.* **2005**, *89*, 4029–4042.

(21) Kusumi, A.; Nakada, C.; Ritchie, K.; Murase, K.; Suzuki, K.; Murakoshi, H.; Kasai, R. S.; Kondo, J.; Fujiwara, T. Paradigm Shift of the Plasma Membrane Concept from the Two-Dimensional Continuum Fluid to the Partitioned Fluid: High-Speed Single-Molecule Tracking of Membrane Molecules. *Annu. Rev. Biophys. Biomol. Struct.* **2005**, *34*, 351–378.

(22) Sezgin, E.; Schneider, F.; Galiani, S.; Urbančič, I.; Waithe, D.; Lagerholm, B. C.; Eggeling, C. Measuring Nanoscale Diffusion Dynamics in Cellular Membranes with Super-Resolution STED–FCS. *Nat. Protoc.* **2019**, *14*, 1054–1083.

(23) Moran, U. Average concentration of a protein in cell; BNID 104520 https://bionumbers.hms.harvard.edu/bionumber.aspx?id=104520 (accessed Sep 24, 2019).

(24) Kask, P.; Günther, R.; Axhausen, P. Statistical Accuracy in Fluorescence Fluctuation Experiments. *Eur. Biophys. J.* **1997**, *25*, 163–169.

(25) Saffarian, S.; Elson, E. L. Statistical Analysis of Fluorescence Correlation Spectroscopy: The Standard Deviation and Bias. *Biophys. J.* **2003**, *84*, 2030–2042.

(26) Qian, H. On the Statistics of Fluorescence Correlation Spectroscopy. *Biophys. Chem.* **1990**, *38*, 49–57.

(27) Wohland, T.; Rigler, R.; Vogel, H. The Standard Deviation in Fluorescence Correlation Spectroscopy. *Biophys. J.* **2001**, *80*, 2987–2999.

(28) Waithe, D.; Schneider, F.; Chojnacki, J.; Clausen, M. P.; Shrestha, D.; de la Serna, J. B.; Eggeling, C. Optimized Processing and Analysis of Conventional Confocal Microscopy Generated Scanning FCS Data. *Methods* **2018**, *140–141*, 62–73.

(29) Böhmer, M.; Wahl, M.; Rahn, H.-J.; Erdmann, R.; Enderlein, J. Time-Resolved Fluorescence Correlation Spectroscopy. *Chem. Phys. Lett.* **2002**, *353*, 439–445.

(30) Isbaner, S.; Karedla, N.; Ruhlandt, D.; Stein, S. C.; Chizhik, A.; Gregor, I.; Enderlein, J. Dead-Time Correction of Fluorescence Lifetime Measurements and Fluorescence Lifetime Imaging. *Opt. Express* **2016**, *24*, 9429–9445.

(31) Manley, S.; Gillette, J. M.; Patterson, G. H.; Shroff, H.; Hess, H. F.; Betzig, E.; Lippincott-Schwartz, J. High-Density Mapping of Single-Molecule Trajectories with Photoactivated Localization Microscopy. *Nat. Methods* **2008**, *5*, 155–157.

(32) Eggeling, C.; Hilbert, M.; Bock, H.; Ringemann, C.; Hofmann, M.; Stiel, A. C.; Andresen, M.; Jakobs, S.; Egner, A.; Schönle, A.; Hell, S. W. Reversible Photoswitching Enables Single-Molecule Fluorescence Fluctuation Spectroscopy at High Molecular Concentration. *Microsc. Res. Tech.* **2007**, *70*, 1003–1009.

(33) Laurence, T. A.; Ly, S.; Bourguet, F.; Fischer, N. O.; Coleman, M. A. Fluorescence Correlation Spectroscopy at Micromolar Concentrations without Optical Nanoconfinement. *J. Phys. Chem. B* **2014**, *118*, 9662–9667.

(34) Laurence, T. A.; Weiss, S. Analytical Chemistry: How to Detect Weak Pairs. *Science*. January 31, 2003, pp 667–668.

(35) Blom, H.; Kastrup, L.; Eggeling, C. Fluorescence Fluctuation Spectroscopy in Reduced Detection Volumes. *Curr. Pharm. Biotechnol.* **2006**, *7*, 51–66.

(36) Foquet, M.; Korlach, J.; Zipfel, W. R.; Webb, W. W.; Craighead, H. G. Focal Volume Confinement by Submicrometer-Sized Fluidic Channels. *Anal. Chem.* **2004**, *76*, 1618–1626.

(37) Wenger, J.; Rigneault, H.; Dintinger, J.; Marguet, D.; Lenne, P. F. Single-Fluorophore Diffusion in a Lipid Membrane over a Subwavelength Aperture. *J. Biol. Phys.* **2006**, *32*, 18–21.

(38) Leutenegger, M.; Gösch, M.; Perentes, A.; Hoffmann, P.; Martin, O. J. F.; Lasser, T. Confining the Sampling Volume for Fluorescence Correlation Spectroscopy Using a Sub-Wavelength Sized Aperture. *Opt. Express* **2006**, *14*, 956.

(39) Kinkhabwala, A. A.; Yu, Z.; Fan, S.; Moerner, W. E. Fluorescence Correlation Spectroscopy at High Concentrations Using Gold Bowtie Nanoantennas. *Chem. Phys.* **2012**, *406*, 3–8.

(40) Manzo, C.; van Zanten, T. S.; Garcia-Parajo, M. F. Nanoscale Fluorescence Correlation Spectroscopy on Intact Living Cell Membranes with NSOM Probes. *Biophys. J.* **2011**, *100*, L8–L10.

(41) Regmi, R.; Winkler, P. M.; Flauraud, V.; Borgman, K. J. E.; Manzo, C.; Brugger, J.; Rigneault, H.; Wenger, J.; García-Parajo, M. F. Planar Optical Nanoantennas Resolve Cholesterol-Dependent Nanoscale Heterogeneities in the Plasma Membrane of Living Cells. *Nano Lett.* **2017**, *17*, 6295–6302.

(42) Kastrup, L.; Blom, H.; Eggeling, C.; Hell, S. W. Fluorescence Fluctuation Spectroscopy in Subdiffraction Focal Volumes. *Phys. Rev. Lett.* **2005**, *94*, 178104.

(43) Barzan, M.; Hajiesmaeilbaigi, F. Investigation the Concentration Effect on the Absorption and Fluorescence Properties of Rhodamine 6G Dye. *Optik (Stuttg).* **2018**, *159*, 157–161.

(44) Honigmann, A.; Mueller, V.; Ta, H.; Schoenle, A.; Sezgin, E.; Hell, S. W.; Eggeling, C. Scanning STED-FCS Reveals Spatiotemporal Heterogeneity of Lipid Interaction in the Plasma Membrane of Living Cells. *Nat. Commun.* **2014**, *5*, 5412.

(45) Hell, S.; Reiner, G.; Cremer, C.; Stelzer, E. H. K. Aberrations in Confocal Fluorescence Microscopy Induced by Mismatches in Refractive Index. *J. Microsc.* **1993**, *169*, 391–405.

(46) Antonello, J.; Burke, D.; Booth, M. J. Aberrations in Stimulated Emission Depletion (STED) Microscopy. *Opt. Commun.* **2017**, *404*, 203–209.

(47) Barbotin, A.; Galiani, S.; Urbančič, I.; Eggeling, C.; Booth, M. J. Adaptive Optics Allows STED-FCS Measurements in the Cytoplasm of Living Cells. *Opt. Express* **2019**, *27*, 23378.

(48) Heine, J.; Wurm, C. A.; Keller-Findeisen, J.; Schönle, A.; Harke, B.; Reuss, M.; Winter, F. R.; Donnert, G. Three Dimensional Live-Cell STED Microscopy at Increased Depth Using a Water Immersion Objective. *Rev. Sci. Instrum.* **2018**, *89*, 053701.

(49) Bacia, K.; Schwille, P. Practical Guidelines for Dual-Color Fluorescence Cross-Correlation Spectroscopy. *Nat. Protoc.* **2007**, *2*, 2842–2856.

(50) Ghosh, A.; Karedla, N.; Thiele, J. C.; Gregor, I.; Enderlein, J. Fluorescence Lifetime Correlation Spectroscopy: Basics and Applications. *Methods* **2018**, *140–141*, 32–39.

(51) Digman, M. A.; Dalal, R.; Horwitz, A. F.; Gratton, E. Mapping the Number of Molecules and Brightness in the Laser Scanning Microscope. *Biophys. J.* **2008**, *94*, 2320–2332.

(52) Digman, M. A.; Brown, C. M.; Sengupta, P.; Wiseman, P. W.; Horwitz, A. R.; Gratton, E. Measuring Fast Dynamics in Solutions and Cells with a Laser Scanning Microscope. *Biophys. J.* **2005**, *89*, 1317–1327.

(53) Wachsmuth, M.; Conrad, C.; Bulkescher, J.; Koch, B.; Mahen, R.; Isokane, M.; Pepperkok, R.; Ellenberg, J. High-Throughput Fluorescence Correlation Spectroscopy Enables Analysis of Proteome Dynamics in Living Cells. *Nat. Biotechnol.* **2015**, *33*, 384–389.

(54) Schneider, F.; Waithe, D.; Clausen, M. P.; Galiani, S.; Koller, T.; Ozhan, G.; Eggeling, C.; Sezgin, E. Diffusion of Lipids and GPI-Anchored Proteins in Actin-Free Plasma Membrane Vesicles Measured by STED-FCS. *Mol. Biol. Cell* **2017**, *28*, 1507–1518.

(55) Sezgin, E.; Kaiser, H.-J.; Baumgart, T.; Schwille, P.; Simons, K.; Levental, I. Elucidating Membrane Structure and Protein Behavior Using Giant Plasma Membrane Vesicles. *Nat. Protoc.* **2012**, *7*, 1042–1051.

(56) Enderlein, J.; Gregor, I.; Patra, D.; Fitter, J. Art and Artefacts of Fluorescence Correlation Spectroscopy. *Curr. Pharm. Biotechnol.* **2004**, *5*, 155–161.

(57) Enderlein, J.; Gregor, I. Using Fluorescence Lifetime for Discriminating Detector Afterpulsing in Fluorescence-Correlation Spectroscopy. *Rev. Sci. Instrum.* **2005**, *76*, 1–5.

Supporting figures

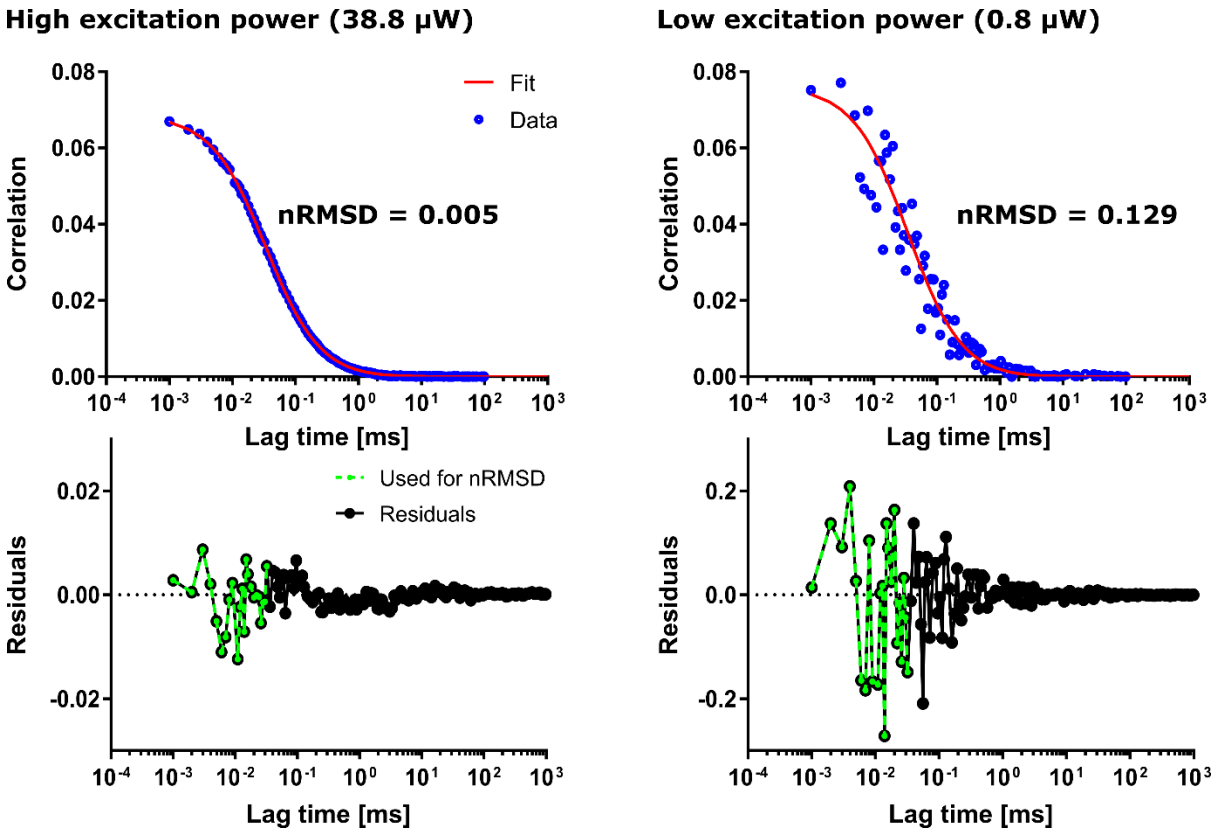

Figure SI 1: Calculation of nRMSD values from the fitting residuals as a measure of the noise level in autocorrelation curves. FCS data of 5 nM Atto655 in aqueous solution acquired at high and low excitation power (38.8 and 0.8 µW, blue data-points in left and right panels, respectively) with respective fits (red curves) and fitting residuals below (black). The residuals highlighted in green (up to the lag time of the fitted transit time) where used for the calculation of the nRMSD value (see Methods). The lower the nRMSD, the better the data quality.

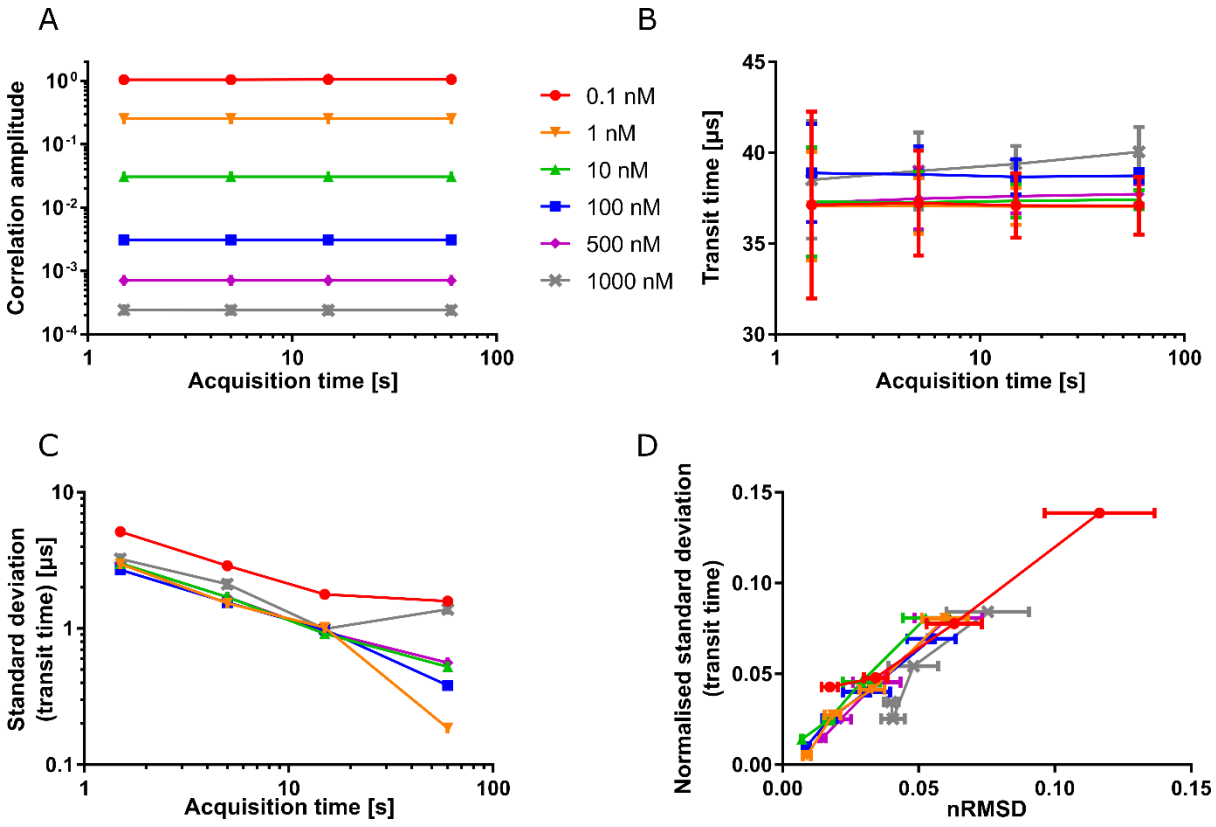

Figure SI 2: Effect of acquisition time on FCS performance at different concentrations of Atto655 in aqueous solution **A** The fitted correlation amplitude, **B** transit time, and **C** standard deviation of the fitted transit time, plotted against the acquisition time. **D** Relative standard deviation of the fitted transit times against the FCS noise level (nRMSD). Measurements were recorded at excitation laser power 15.4 µW and acquisition time 60 s, and then chopped into shorter intervals, as indicated.

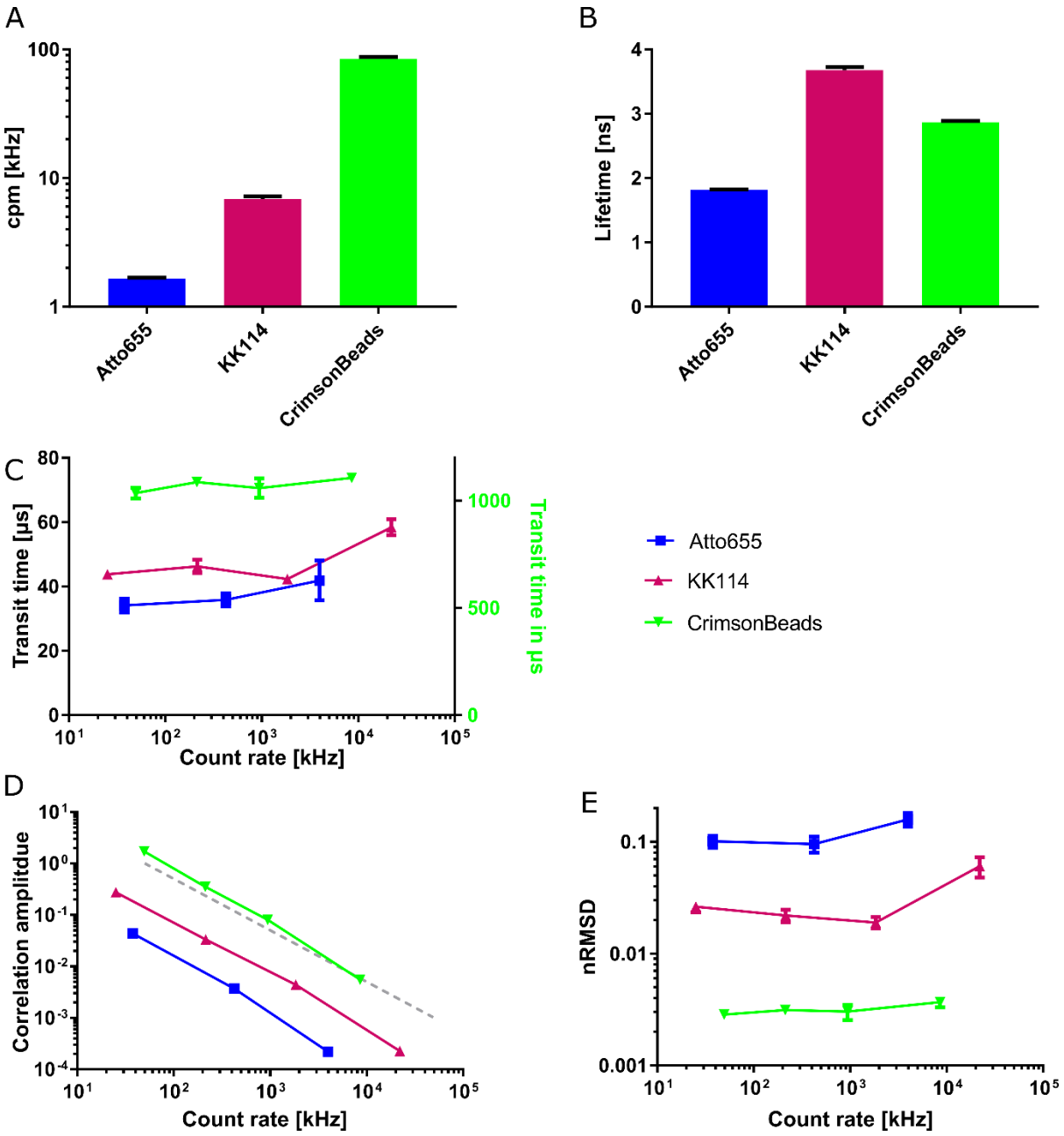

Figure SI 3: Influence of molecular brightness and fluorescence lifetime of dyes on performance in FCS at different count rates. **A** Counts per molecule and **B** fluorescence lifetime from single exponential fits to TCSPC histograms, for aqueous solutions of Atto655, KK114 (Abberior STAR Red) and Crimson Beads **C** Fitted transit time, **D** Correlation amplitude, and **E** FCS noise level (nRMSD) obtained for various concentrations of Atto655 (0.01, 0.1, and 1 µM), KK114 (0.01, 0.1, 1, and 10 µM) and Crimson Beads (1:2000, 1:500, 1:100, and 1:10 dilutions of the purchased stock solution), resulting in different count rates. Excitation laser power 1.5 µW, acquisition time 60 s, data-points represent averages and standard deviations of at least 3 measurements. The grey dashed line in **D** represents a linear relationship. Average nRMSD values from panel E were used for the inset in Figure 2E.

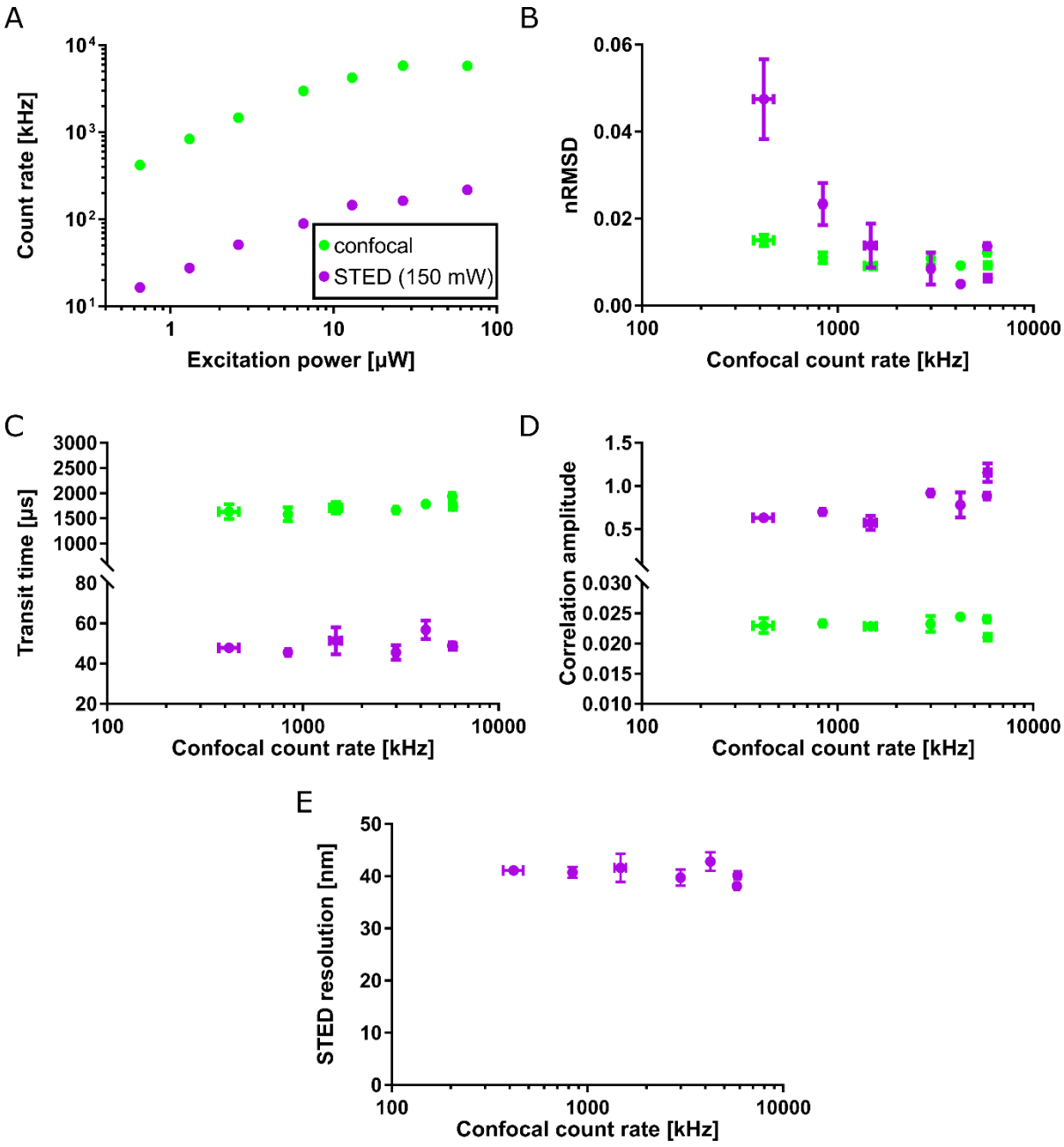

Figure SI 4: STED-FCS measurements of fluorescent Abberior STAR Red- DPPE in a DOPC SLB – acquired at varying excitation laser powers from 0.7 µW to 66 µW. **A** Change in confocal (green) and STED (purple) count rate when varying the excitation power. **B** The FCS noise level (nRMSD), **C** fitted transit times, **D** correlation amplitude, and **E** apparent STED resolution plotted against confocal count rate for confocal (green) and STED recordings (purple). Acquisition time 15 s, depletion laser power 150 mW. Data-points represent averages and standard deviations of at least 3 measurements.

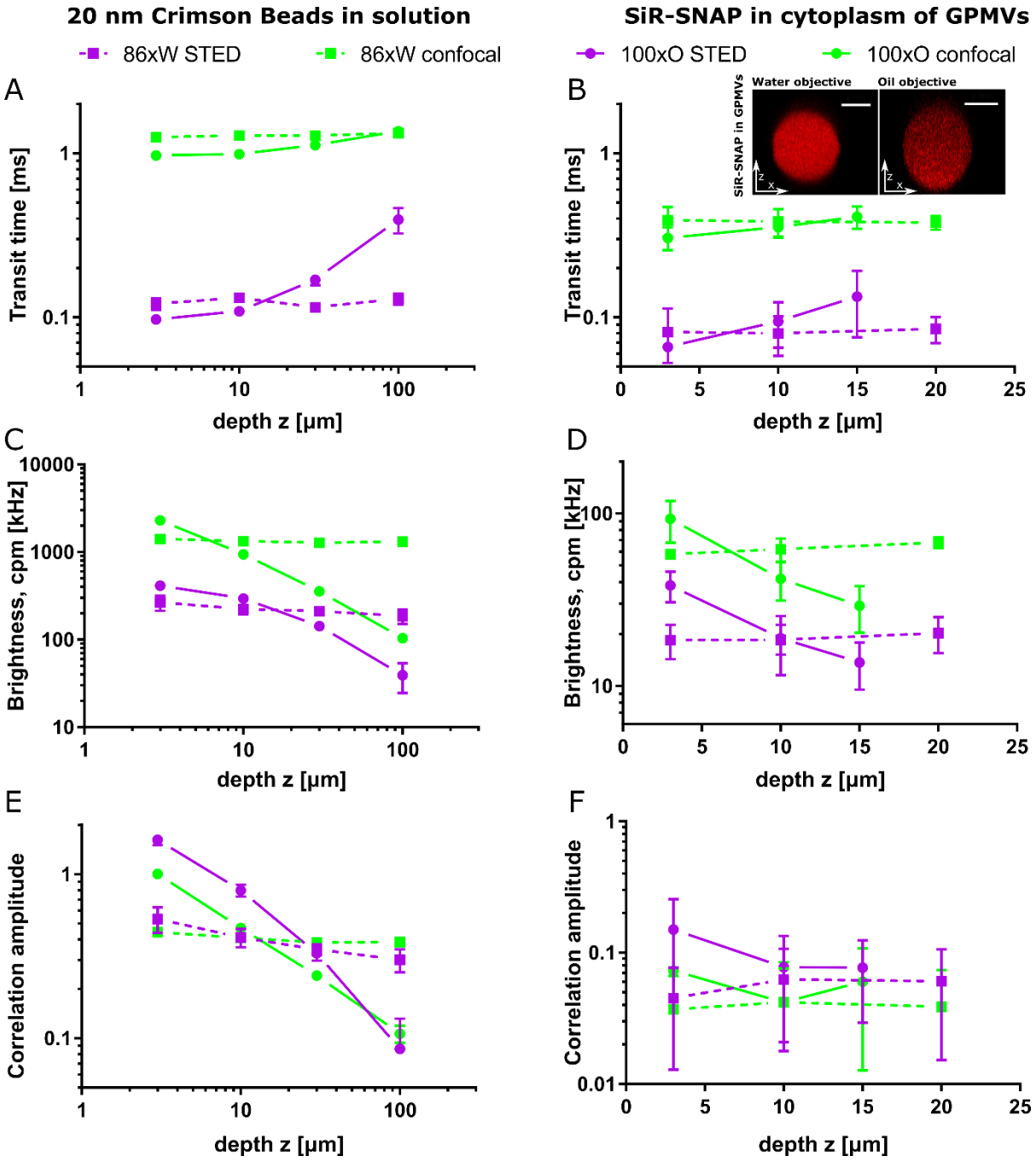

Figure SI 5: Performance of (STED-)FCS depends on objective and depth. (STED-)FCS experiments at different focal depth (z) for 20 nm Crimson beads in water **(left panel A, C, E)** and SiR-SNAP in cytoplasm of immobilised CHO GPMVs **(right panel B,D,F)** using a 100x oil- (circles, solid lines) and 86x water-immersion objective (squares, dashed lines). **A,B** The transit times, **C,D** molecular brightness (cpm) and **E,F** correlation amplitude determined from measurements at different focal depths in confocal (green) and STED mode (purple). Excitation laser power 8.9 µW, depletion laser powers 140 and 56 mW for crimson beads and SiR-SNAP, respectively, acquisition time 20 s. All data points are averages and standard deviations from at least 3 measurements. The inset in **B** shows confocal images of axial cross-sections of CHO GPMVs with SiR-SNAP in the cytoplasm.

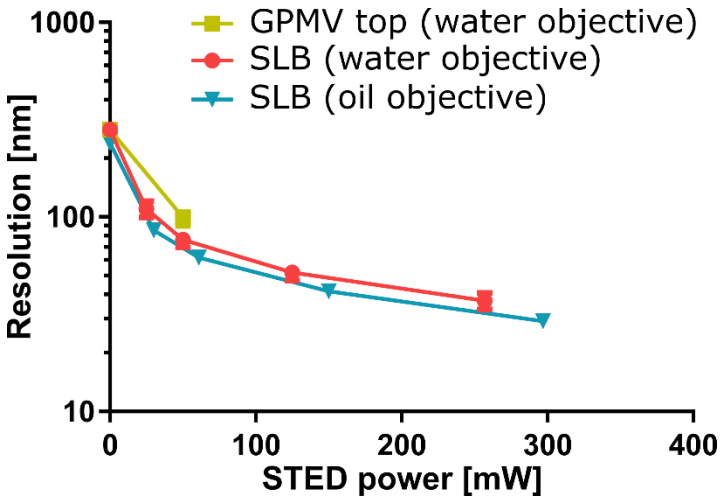

Figure SI 6: STED-FCS resolution calibration using SLBs (Abberior STAR Red-DPPE in DOPC) with oil- (blue) and water-immersion (orange) objectives, compared to the resolution obtained from the top membrane of CHO GPMVs (labelled with freely diffusing Abberior STAR Red-PEG-Cholesterol with a water-immersion objective (yellow)). Excitation power was 2.3 µW and depletion power was 125 mW, acquisition time 15 s. From at least three measurements per condition, the average value and their standard deviation is shown.

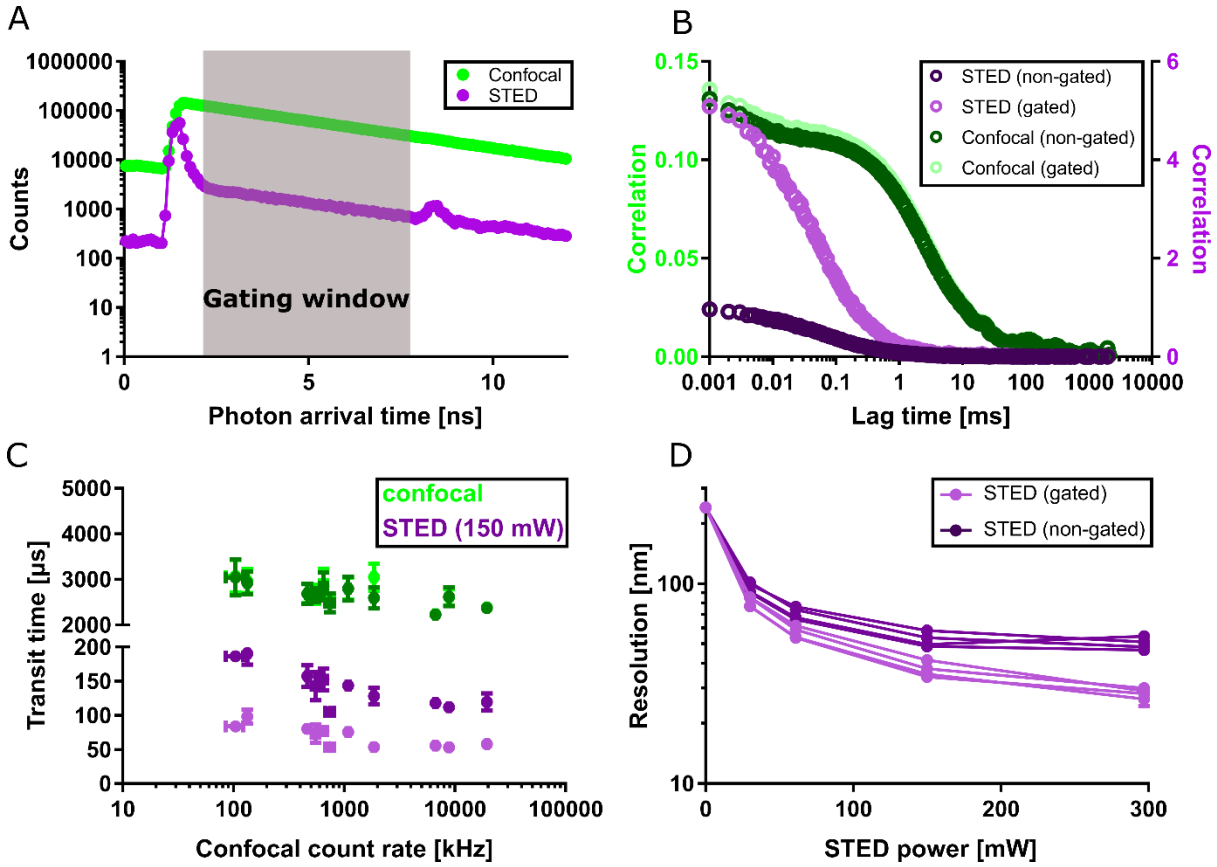

Figure SI 7: Influence of time gating in STED-FCS **A** Time correlated single photon counting (TCSPC) histograms of photon arrival times for an exemplary confocal (green) and STED-FCS measurement (purple, 150 mW depletion power) on a DOPC SLB labelled with Abberior STAR Red - DPPE. The gating window (grey area) was chosen to exclude confocal contributions to the STED-FCS correlation and to exclude the bump from the white light laser reflection in our system. **B** Exemplary correlation curves, and **C** average fitted transit times for confocal (green) and STED recordings (purple), analysed with and without gating applied (lighter and darker symbols, respectively). **D** Apparent resolution (i.e., diameter of the effective observation spot) as calculated from confocal and STED transit times for gated (light purple) and non-gated (dark purple) data acquired at different STED laser powers. Measurements of 15 s were acquired at 2.3 µW excitation laser power. In panels C and D, average and standard deviation of three measurements are shown.